CrossMark

ORIGINAL PAPER

On the Gas Heating Mechanism for the Fast Anode Arc Reattachment in a Non-transferred Arc Plasma Torch Operating with Nitrogen Gas in the Restrike Mode

L. Prevosto[1] · H. Kelly[1,2] · B. Mancinelli[1] · J. C. Chamorro[1]

Abstract The present work provides a detailed kinetic analysis of the time-resolved dynamics of the gas heating during the arc reattachment in nitrogen gas in order to understand the main processes leading to such a fast reattachment. The model includes gas heating due to the relaxation of the energy stored in the vibrational as well as the electronic modes of the molecules. The results show that the anode arc reattachment is essentiality a threshold process, corresponding to a reduced electric field value of $E/N \sim 40$ Td for the plasma discharge conditions considered in this work. The arc reattachment is triggered by a vibrational instability whose development requires a time of the order of 100 μs. For $E/N < 80$–100 Td, most of the electron energy is transferred to gas heating through the mechanism of vibrational–translational relaxation. For larger values of E/N the electronic–translational energy relaxation mechanism produces a further intensification of the gas heating. The sharp increase of the gas heating rate during the last few μs of the vibrational instability give rises to a sudden transition from a diffuse (glow-like) discharge to a constricted arc with a high current density ($\sim 10^7$ A/m^2). This sudden increase in the current density gives rise to a new anode attachment closer to the cathode (where the voltage drop between the original arc and the anode is the largest) thus causing the decay of the old arc spot.

Keywords Anode arc reattachment · Vibrational instability · Fast gas heating · Plasma torches

✉ L. Prevosto
   prevosto@waycom.com.ar

1 Grupo de Descargas Eléctricas, Departamento Ing. Electromecánica, Facultad Regional Venado Tuerto (UTN), Laprida 651, Venado Tuerto, 2600 Santa Fe, Argentina

2 Instituto de Física del Plasma (CONICET), Facultad de Ciencias Exactas y Naturales (UBA), Ciudad Universitaria Pab. I, 1428 Buenos Aires, Argentina

 Springer

Introduction

Direct current (dc) non-transferred arc plasma torches are used in a number of applications like spray coatings, material synthesis, and waste treatment. Standard dc non-transferred plasma torches are characterized by a central rod-shape cathode and a concentric water-cooled copper anode. The arc connects the cathode tip to some point on the anode wall, crossing through the cold gas boundary layer that covers such wall. Typical torch currents are in the range of a few hundred amperes [1, 2].

Unlike non-transferred arcs with fixed minimal lengths [3], the anode attachment location in a non-transferred arc is usually in motion, thus inducing arc voltage fluctuations. Three distinctive modes have been reported for the arc voltage fluctuations: the steady mode, rather detrimental for the anode life time because the anodic attached spot remains almost fixed in position; the takeover mode, obtained mainly with mono-atomic gases in which the anode attached spot presents a small amplitude oscillating motion; and the restrike mode, corresponding to diatomic gases or their mixtures, in which the spot expands along the anode moving away from the cathode (stretching the arc) until a new arc appears closer to the cathode and the original arc decays, giving place to an expanding movement of the new arc [4]. In the steady mode, the arc voltage remains almost constant. In the takeover mode, the arc voltage presents a small oscillation (of the order of a few volts). Finally, the restrike mode is characterized by a saw-tooth-like shape of the arc voltage with quasi-periodic fluctuations, being the amplitude of these fluctuations as high as 40 % of the time-averaged arc voltage. A large range of plasma operating conditions used for plasma spraying matches this last condition [2]. Figure 1 shows a typical arc voltage waveform corresponding to a non-transferred dc plasma torch operated at 100 A with a nitrogen flow rate of 25 Nl/min (more details on the employed torch can be found elsewhere [5]). Each sharp voltage drop with a time scale of the order of 1 μs (inset of Fig. 1) corresponds to the creation of a new arc root (lasting for times between 50 and 200 μs).

The physical mechanism of the anode attachment restrike is well understood. The anode arc column which connects the main arc column and the anode wall is pushed forward by the gas flow thus elongating the arc length and increasing the arc voltage drop until the cold boundary layer "electrically breaks", giving rise to a new anode attachment closer to

Fig. 1 Typical arc voltage waveform corresponding to the restrike mode in a dc plasma torch. The sharp voltage drop corresponding to the restrike process is showed in the *inset*
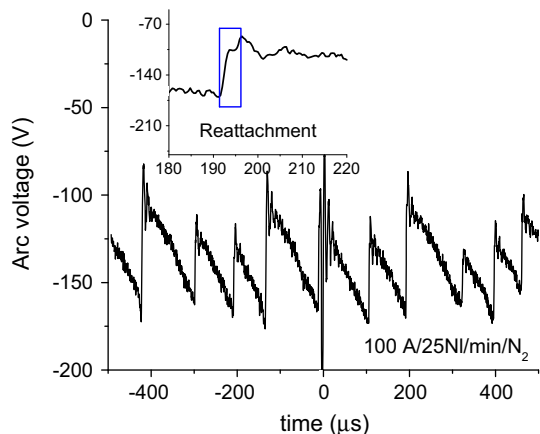
the cathode (where the voltage difference between the arc and the anode is largest). As the new configuration of the arc has a lower voltage drop, the new attachment causes a decay of the old one, being again dragged away by the flow [4]. However, the physical mechanism driving the fast anode arc reattachment process (time scale of the order of μs) is less clear. There are no plasma torch models free of artificial assumptions (e.g. by imposing an electrically conducting channel between the arc and the anode) to simulate the reattachment process in the restrike operating mode [6, 7].

Experimental observations [8] have shown that a relatively small fraction of the main arc current (of about 10 %) flows upstream of the arc attachment trough a dark anode boundary layer; thus indicating there the existence of a non-thermal diffuse (glow-like) discharge. Such a kind of high-pressure discharge tends to be unstable and an increase in the current usually produces a sudden transition to an arc state characterized by a large increase in the current density and a considerable decrease in the discharge voltage. A universal mechanism for the transition from diffuse to contracted or localized current flow is the so called thermal instability [9], in which a local increase of the translational gas temperature causes a local decrease of its density, leading to an increase of the reduced electric field and of the electron temperature; this increase of electron temperature results in an enlargement of the ionization and of the electron density. This type of instability was recently considered in [10] for the anode reattachment process but without taking into account the underlying physical processes leading to the gas heating due to the energetic electrons.

The gas temperature in a plasma discharge is largely determined by the rate of energy transfer from the electrons to the gas heavy particle. A significant difference is observed in the rate of energy transfer between the electrons and neutral atoms and electrons and neutral molecules. In atomic gases, the gas temperature increase is caused mainly by energy transfer from elastic collisions between electrons and atoms, the so-called $e–T$ (electron–translational) energy transfer. Because of the large mass difference between these particles, this is a very inefficient mechanism. For reduced electric fields, $E/N > 20$ Td (E is the electric field strength, N the gas number density and 1 Td $\equiv 10^{-21}$ Vm^2); the fractional electron power transferred in elastic collisions to gas heating is less than a few times 10^{-3} [11]. In molecular gases, electrons can transfer energy to additional intermediate internal energy modes of the molecule such as vibrational and rotational energy. Since the typical characteristic vibrational energy of the molecules (0.2–0.5 eV) is comparable to typical electron temperatures (of about 1 eV) at $20 < E/N < 80$ Td, most of the electron energy is transferred to vibrational modes, $e–V$, and then to gas temperature mainly through the mechanism of $V–T$ relaxation [11]. Since the rates of $e–V$ and $V–T$ energy transfer mechanisms are significantly larger than $e–T$, molecular gases typically have higher heating rates and are more susceptible to thermalization. This is due to the strong exponential dependence of the $V–T$ relaxation rate coefficient on the gas temperature. Even small increases of the gas temperature lead to a significant increase of the $V–T$ relaxation rate, intensification of heating, and then to a further growth of the gas temperature. This is the vibrational instability mode sometimes called the "thermal explosion" of vibrational reservoir [12]. This process takes a sufficiently long time ($\gg 1$ μs in nitrogen gas at atmospheric pressure). Higher electric fields, $E/N > 80–100$ Td, produce a more efficient energy transfer from electrons to electronic states than $e–V$ [11, 12]. In turn, the electronic energy relaxation mechanism, $E–T$ can be very fast compared to the $V–T$ relaxation time (the so called "fast gas heating" [13–16]). In pure molecular nitrogen the mechanism of fast gas heating was mainly ascribed to self-quenching reactions of the metastable electronic state $N_2(A^3\sum_u^+)$ [17].

The present work provides a detailed kinetic analysis of the time-resolved dynamics of the gas heating during the arc reattachment in nitrogen gas in order to understand the main

processes leading to such a fast reattachment. The model includes gas heating due to the relaxation of the energy stored in the vibrational as well as the electronic modes of the molecules. The results of the calculations are compared with the available experimental data on arc voltage waveforms.

Model of the Discharge

Kinetic Model

The purpose of this discharge model was to study possible mechanisms of fast transfer of electron energy into thermal energy (gas heating) in a non-equilibrium high-pressure plasma discharge formed in moderate reduced electric field values ($\sim$40–120 Td). The model includes the balance equations for the most important neutral and charged species present in the discharge together with the equations describing the mean vibrational energy of the $N_2(X^1\sum_g^+, v)$ molecules and the gas temperature. The considered species for pure nitrogen are the vibrational manifold of ground state molecules $N_2(X^1\sum_g^+, v)$, the electronic excited states of nitrogen molecules and atoms $N_2(A^3\sum_u^+)$, $N_2(B^3\Pi_g)$, $N_2(a'^1\sum_u^-)$, $N_2(C^3\Pi_u)$, $N(^2D)$ and $N(^2P)$, the atomic ground state $N(^4S)$, the positive ions N_4^+, N_2^+ and N^+; and the electrons (e).

The included reactions are summarized in Table 1, where the gas temperature (T_g) and the effective electron temperature (T_e) units are in K. The dependences on the reduced electric field of the rate coefficients for electron-impact excitation (R1–R4), dissociation (R5) and ionization (R6–R7) as well as the effective electron temperature T_e and the electron mobility (μ_e) were calculated by solving the electron Boltzmann equation in the classical two-term approximation with the BOLSIG+ code [18]. The rate coefficients for stepwise ionization from $N_2(A^3\sum_u^+)$ and $N_2(a'^1\sum_u^-)$ (R8–R9) have been calculated from the cross section data reported in [19]. The electronic excitation by electron impact was assumed to occur only from the vibrational ground state $N_2(X^1\sum_g^+, 0)$ [the rate coefficients for electronic excitation, dissociation and ionization from $N_2(X^1\sum_g^+, v)$ were assumed to be the same as those from $N_2(X^1\sum_g^+, 0)$]. Although the rates of electronic excitation, dissociation, and ionization can be affected by this approximation, the electron energy transfer to the vibrational manifold is not much affected by making this assumption [17]. The rate coefficients for excitation, dissociation and ionization calculated with the use of the BOLSIG+ code (for conditions of vibrationally non-excited gas) were corrected by means of the factor [11, 20]

$$F = \exp\left[\frac{C\exp(-\hbar\omega/(kT_v))}{(E/N)^2}\right], \tag{1}$$

that takes into account the increases of the electron energy due to super-elastic collisions with vibrationally excited nitrogen molecules. In Eq. (1) $C = 6.5 \times 10^3$ Td^2 [20], k is the Boltzmann constant and $\hbar\omega$ and T_v are the vibrational quantum (=0.29 eV) and the vibrational temperature of the nitrogen molecule; respectively. The mean vibrational energy of the nitrogen molecule (ε_v) was related to T_v as $\varepsilon_v = \hbar\omega/[\exp(\hbar\omega/(kT_v)) - 1]$. The dependences on E/N of the rate coefficients for electron-impact excitation (R1–R4) and dissociation (R5), together with the rate coefficients for direct electron impact ionization (R6–R7) as well as the stepwise ionization (R8–R9), are shown in Fig. 2a, b, respectively. The calculations correspond in this case to a vibrationally excited nitrogen

Table 1 Reactions considered in the kinetic model

No.	Reaction	Rate coefficient [m^3/s or m^6/s (*)]	References
Electron-impact excitation			
(R1)	e + N$_2$(X, v) → e + N$_2$(A)	$k_1 = f(E/N)\ F$	See text
(R2)	e + N$_2$(X, v) → e + N$_2$(B)	$k_2 = f(E/N)\ F$	See text
(R3)	e + N$_2$(X, v) → e + N$_2$(a)	$k_3 = f(E/N)\ F$	See text
(R4)	e + N$_2$(X, v) → e + N$_2$(C)	$k_4 = f(E/N)\ F$	See text
Electron-impact dissociation			
(R5)	e + N$_2$(X, v) → N$_2$(E* = 13 eV) N$_2$(E* = 13 eV) → N(^{4}S) + N(^{2}D)	$k_5 = f(E/N)\ F$	See text
Direct electron-impact ionization			
(R6)	e + N$_2$(X, v) → e + e + N$_2^+$	$k_6 = f(E/N)\ F$	See text
(R7)	e + N(4S) → e + e + N$^+$	$k_7 = f(E/N)\ F$	See text
Stepwise ionization			
(R8)	e + N$_2$(A) → e + e + N$_2^+$	$k_8 = f(E/N)\ F$	See text
(R9)	e + N$_2$(a) → e + e + N$_2^+$	$k_9 = f(E/N)\ F$	See text
Associative ionization			
(R10)	N$_2$(A) + N$_2$(a) → e + N$_4^+$	$k_{10} = 5.0 \times 10^{-17}$	[27]
(R11)	N$_2$(a) + N$_2$(a) → e + N$_4^+$	$k_{11} = 2.0 \times 10^{-16}$	[27]
(R12)	N(^{2}P) + N(^{2}P) → e + N$_2^+$	$k_{12} = 3.0 \times 10^{-17}$	[28]
Quenching of electronically excited particles			
(R13)	N$_2$(A) + N$_2$(A) → N$_2$(X, v) + N$_2$(B)	$k_{13} = 1.1 \times 10^{-15}$	[29]
(R14)	N$_2$(A) + N$_2$(A) → N$_2$(X, v) + N$_2$(C)	$k_{14} = 3.0 \times 10^{-16}$	[30]
(R15)	N$_2$(B) + N$_2$(X, v) → N$_2$(A) + N$_2$(X, v)	$k_{15} = 3.0 \times 10^{-17}$	[31]
(R16)	N$_2$(C) → N$_2$(B) + hv	$v_{16} = 3.0 \times 10^7$ s^{-1}	[32]
(R17)	N(^{2}D) + N$_2$(X, 0) → N$_2$(X, 0) + N(^{4}S)	$k_{17} = 6.0 \times 10^{-21}$	[32]
(R18)	N$_2$(A) + N(^{4}S) → N$_2$(X, v) + N(^{2}P)	$k_{18} = 4.0 \times 10^{-17}(300/T_g)^{2/3}$	[21]
Electron–ion recombination			
(R19)	e + N$_2^+$ → N(^{4}S) + N(^{2}D)	$k_{19} = 2.0 \times 10^{-13}(300/T_e)^{1/2}$	[32]
(R20)	e + N$_4^+$ → N$_2$(X, v) + N$_2$(C)	$k_{20} = 2.0 \times 10^{-12}(300/T_e)^{1/2}$	[32]
(R21)	e + e + N$_2^+$ → e + N$_2$(X, v)	$k_{21} = 1.0 \times 10^{-31}(300/T_e)^{9/2}$ (*)	[32]
(R22)	e + e + N$^+$ → e + N(^{4}S)	$k_{22} = 2.0 \times 10^{-39}(10^4/T_e)^{6.04}$ (*)	[33]

gas at $T_v = 6000$ K, which is a typical vibrational state for a high-pressure non-equilibrium discharge in nitrogen gas in moderate reduced electric field values.

The balance equations for the active species (evaluated in a local approximation) were solved for the densities of N$_2$(A$^3\sum_u^+$), N$_2$(a$^{'1}\sum_u^-$), N(^{2}D), N(^{2}P), N(^{4}S), N$_4^+$, N$^+$ and electrons.

$$\frac{\partial}{\partial t}([N_2(A)]) = [N_e][N_2(X)](k_1 + k_2 + k_4) - k_8[N_e][N_2(A)] - k_{10}[N_2(a)][N_2(A)]$$
$$- [N_2(A)]^2(k_{13} + k_{14}) - k_{18}[N(^4S)][N_2(A)], \tag{2}$$

Fig. 2 **a** Rate coefficients for electron-impact excitation (R1–R4) and dissociation (R5) vs the reduced electric field. **b** Rate coefficients for direct electron impact ionization (R6–R7) and stepwise ionization (R8–R9) versus the reduced electric field. The calculations correspond to a nitrogen gas at $T_v = 6000$ K
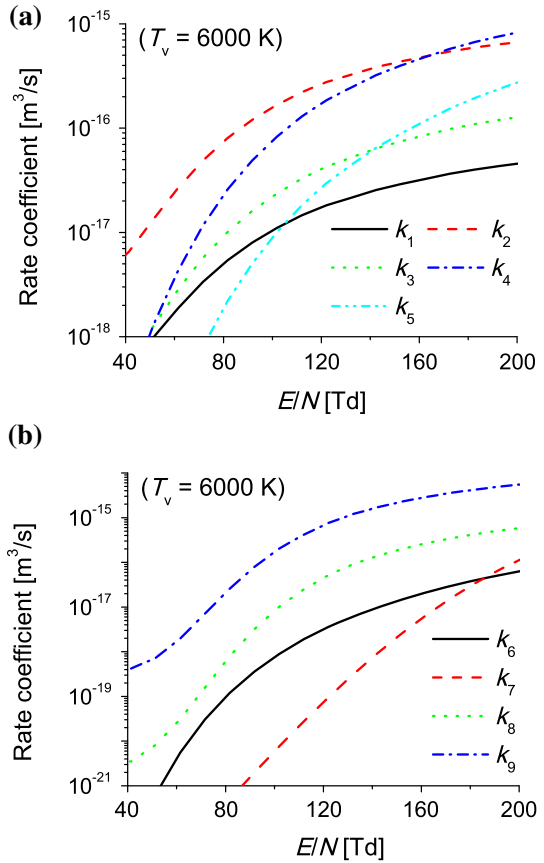
$$\frac{\partial}{\partial t}([\mathrm{N_2}(a)]) = k_3[\mathrm{N}_e][\mathrm{N_2}(X)] - k_9[\mathrm{N}_e][\mathrm{N_2}(a)] \\ - k_{10}[\mathrm{N_2}(a)][\mathrm{N_2}(A)] - k_{11}[\mathrm{N_2}(a)]^2, \tag{3}$$

$$\frac{\partial}{\partial t}\left([\mathrm{N}(^2\mathrm{D})]\right) = k_5[\mathrm{N}_e][\mathrm{N_2}(X)] - k_{17}\left[\mathrm{N}(^2\mathrm{D})\right][\mathrm{N_2}(X,0)] + k_{19}[\mathrm{N}_e]\left[\mathrm{N_2^+}\right], \tag{4}$$

$$\frac{\partial}{\partial t}\left([\mathrm{N_2}(^2\mathrm{P})]\right) = -k_{12}\left[\mathrm{N_2}(^2\mathrm{P})\right]^2 + k_{18}\left[\mathrm{N}(^4\mathrm{S})\right][\mathrm{N_2}(A)], \tag{5}$$

$$\frac{\partial}{\partial t}\left([\mathrm{N}(^4\mathrm{S})]\right) = k_5[\mathrm{N}_e][\mathrm{N_2}(X)] - k_7[\mathrm{N}_e]\left[\mathrm{N}(^4\mathrm{S})\right] + k_{17}\left[\mathrm{N}(^2\mathrm{D})\right][\mathrm{N_2}(X,0)] \\ - k_{18}\left[\mathrm{N}(^4\mathrm{S})\right][\mathrm{N_2}(A)] + k_{19}[\mathrm{N}_e]\left[\mathrm{N_2^+}\right] + k_{22}[\mathrm{N}_e]^2[\mathrm{N^+}], \tag{6}$$

$$\frac{\partial}{\partial t}\left([\mathrm{N_4^+}]\right) = k_{10}[\mathrm{N_2}(a)][\mathrm{N_2}(A)] + k_{11}[\mathrm{N_2}(a)]^2 - k_{20}[\mathrm{N}_e]\left[\mathrm{N_4^+}\right], \tag{7}$$

$$\frac{\partial}{\partial t}([\mathrm{N^+}]) = k_7\left[\mathrm{N}(^4\mathrm{S})\right][\mathrm{N}_e] - k_{22}[\mathrm{N}_e]^2[\mathrm{N^+}], \tag{8}$$

$$\frac{\partial}{\partial t}([N_e]) = k_6[N_e][N_2(X)] + k_7[N_e][N(^4S)] + k_8[N_e][N_2(A)]$$
$$+ k_9[N_e][N_2(a)] + k_{10}[N_2(A)][N_2(a)] + k_{11}[N_2(a)]^2 + k_{12}[N(^2P)]^2 \tag{9}$$
$$- k_{19}[N_e][N_2^+] - k_{20}[N_e][N_4^+] - k_{21}[N_e]^2[N_2^+] - k_{22}[N_e]^2[N^+],$$

The density of N_2^+ positive ions was obtained from the condition of charge conservation, the density of the dominant specie $N_2(X^1\sum_g^+, v)$ was obtained from the condition that the total pressure be equal to the atmospheric one. The $N_2(B^3\Pi_g)$ and $N_2(C^3\Pi_u)$ electronic states were assumed to decay instantaneously, since according to R15 and R16, respectively, their quenching rates are much shorter than 1 μs in atmospheric pressure gases. Thus, the rate for the production of $N_2(A^3\sum_u^+)$ state by cascading was assumed to be equal to the sum of the rates for the production (by electron impact) of the $N_2(B^3\Pi_g)$ and $N_2(C^3\Pi_u)$ states. By making this assumption, the populations of the $N_2(B^3\Pi_g)$ and $N_2(C^3\Pi_u)$ electronic states do not need to be computed directly [17].

Vibrational Model

The dynamics of the mean vibrational energy of the $N_2(X^1\sum_g^+, v)$ molecule was described by the equation

$$\frac{\partial}{\partial t}([N_2(X)]\varepsilon_v) = Q_{eV} - Q_{VT} - Q_{VV}, \tag{10}$$

where the square brackets indicate particle number density. The terms Q_{eV}, Q_{VT}, and Q_{VV} account for the rate of electron energy transfer to the vibrational levels (e–V process), for the rate of V–T relaxation of nitrogen molecules from the first ($v = 1$) vibrational level and for the rate of an-harmonic (V–V)–T relaxation of nitrogen molecules from the upper vibrational levels; respectively. For the calculation of Q_{eV} only the first eight levels of the $N_2(X^1\sum_g^+, v)$ molecule have been considered [17]

$$e + N_2\left(X^1\Sigma_g^+, v\right) \rightarrow e + N_2\left(X^1\Sigma_g^+, w\right), \tag{11}$$
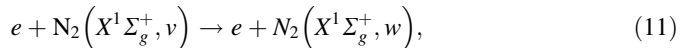
where $0 \leq v \leq 8$ and $0 \leq w \leq 8$. The rate coefficients for the e–V process between excited vibrational levels $k_{eV}(v \rightarrow v + n)$ were scaled as [21]
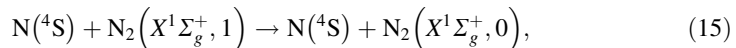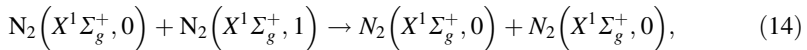
$$k_{eV}(v \rightarrow v + n) = k_{eV}(0 \rightarrow n)(1 + 0.05v)^{-1}, \tag{12}$$

and the rate coefficients from the vibrational ground state were calculated using the BOLSIG+. The dependence of Q_{eV} on T_v was taken into account by calculating the total energy stored in the vibrational modes [in according to processes (11)], but subtracting the vibrational energy losses by super-elastic collisions, considered by the non-equilibrium factor F presented in (1). These collisions increase the energy stored in the electronic states involving excitation of electronic states (R1–R4), dissociation (R5) and ionization (R6–R7) including metastables (R8–R9). Thus, the term Q_{eV} describing the e–V process was calculated as

$$Q_{eV} = \left[[N_e] \sum_{v=0}^{7} [N_2(X, v)] \sum_{n=1}^{8-v} v\hbar\omega k_{eV}(v \rightarrow v + n) \right]$$
$$- \frac{F-1}{F} [N_e][N_2(X, v)](k_1 E_A + k_2 E_B + k_3 E_a + k_4 E_C + k_5 E^* + k_6 I_{N_2})$$
$$- \frac{F-1}{F} [N_e] \left([N(^4S)]k_7 I_N + [N_2(A)k_8(I_{N_2} - E_A) + N_2(a)k_9(I_{N_2} - E_a)] \right), \quad (13)$$

where it was assumed that the population of the first vibrational levels ($v \leq 8$) closely follows a Boltzmann distribution with temperature T_v [17]. ($E_A = 6.17$ eV, $E_B = 7.35$ eV, $E_a = 8.40$ eV and $E_C = 11.03$ eV; are the excitation energy of the electronic states A, B, a and C, respectively; $E^* = 13$ eV is the excitation energy of the pre-dissociation state of the molecule, and $I_{N_2} = 15.58$ eV and $I_N = 14.6$ eV are the ionization energy of the ground states molecules and atoms, respectively).

The calculation of Q_{VT} included $V–T$ relaxation of $N_2(X^1\sum_g^+, v)$ by collisions with ground state molecules as well as with dissociated ground state atoms, in according to the following processes

$$N_2\left(X^1\Sigma_g^+, 0\right) + N_2\left(X^1\Sigma_g^+, 1\right) \rightarrow N_2\left(X^1\Sigma_g^+, 0\right) + N_2\left(X^1\Sigma_g^+, 0\right), \quad (14)$$

$$N\left(^4S\right) + N_2\left(X^1\Sigma_g^+, 1\right) \rightarrow N\left(^4S\right) + N_2\left(X^1\Sigma_g^+, 0\right), \quad (15)$$

being the corresponding rate coefficients [11]

$$k_{N_2}^{10}\left(m^3/s\right) = 7.8 \times 10^{-18} \exp\left[-\frac{218}{T_g^{1/3}} + \frac{690}{T_g}\right]\left(1 - \exp\left(-\frac{\hbar\omega}{kT_g}\right)\right)^{-1}, \quad (16)$$

$$k_N^{10}\left(m^3/s\right) = 2.3 \times 10^{-19} \exp\left[-\frac{1280}{T_g}\right] + 2.7 \times 10^{-17} \exp\left[-\frac{10840}{T_g}\right]. \quad (17)$$

The term Q_{VT} describing the $V–T$ process was calculated as

$$Q_{VT} = [N_2(X)] \frac{\varepsilon_v - \varepsilon_v(T_g)}{\tau_{VT}}, \quad (18)$$

where $\varepsilon_v(T_g)$ is the equilibrium value of nitrogen vibrational energy and τ_{VT} is the time scale of the $V–T$ relaxation by molecules and atoms collisions [11]

$$\tau_{VT} = \frac{1}{\left(1 - \exp\left[-\frac{\hbar\omega}{kT_g}\right]\right)\left(k_{N_2}^{10}[N_2(X, 0)] + k_N^{10}[N(^4S)]\right)}. \quad (19)$$

The an-harmonic heating [$(V–V)–T$ energy transfer] was calculated as

$$Q_{VV} = \hbar\omega\Pi, \quad (20)$$

where $\Pi = \Pi(T_g, T_v)$ is the flow of vibrational quanta in the vibrational energy domain [22].

Gas Heating Model

It was assumed that the energy stored in translational and rotational modes instantly reach equilibrium because translational to translational $(T–T)$ relaxation occurs within a few collisions between the heavy species and rotational to translational $(R–T)$ relaxation takes place within a few ten molecular collisions [11]. Therefore, it was assumed that the translational and rotational temperatures were equilibrated in the discharge. The dynamics of the translational temperature was described by the equation

$$\frac{\partial}{\partial t}\left(\left\{\frac{5}{2}([N_2(X)] + [N_2(A)] + [N_2(B)] + [N_2(C)] + [N_2(a')] + [N_2^+])\right.\right.$$
$$\left.\left. + \frac{6}{2}[N_4^+] + \frac{3}{2}([N^+] + [N(^4S)] + [N(^2D)] + [N(^2P)])\right\}kT_g\right) \tag{21}$$
$$= Q_R + Q_{VT} + Q_{VV} - Q_C,$$

where Q_R and Q_C account for the gas heating rate from chemical reactions and for the gas cooling; respectively. In this model the heat released in the dissociation processes by electron impact (R5), in the reactions of quenching of metastable electronically excited $N_2(A^3\sum_u^+)$ states (R13–R14) and during the electron–ion recombination processes (R19–R20) was taken into account for the calculation of Q_R. The dissociation of the nitrogen molecules goes through excitation of these molecules by an electron impact and following pre-dissociation via electronically excited states [13, 14]. For the reaction R5 the difference between the excitation energy ($E^* = 13$ eV) of the pre-dissociation sate of the molecule and its dissociation threshold [12.1 eV with products $N(^4S) + N(^2D)$] goes into heating. Thus, the energy going into heating is $\Delta E_5 = 0.9$ eV [14]. For the reaction R13 the energy excess is 4.18 eV; about half of this energy corresponds to the energy in the $N_2(X^1\sum_g^+, 8)$ level into which the molecule is assumed to decay, while the remaining $\Delta E_{13} = 2.0$ eV goes into heating [17]. For the reaction R14 about 60 % of the energy excess (1.01 eV) goes in the $N_2(X^1\sum_g^+, 2)$, while the remaining $\Delta E_{14} = 0.4$ eV is assumed to go into heating [17]. Finally, the energy which goes to gas heating due to reactions R19 and R20 is $\Delta E_{19} = 3.44$ eV [15] and $\Delta E_{20} = 3.5$ eV [23], respectively. Hence, the term Q_R describing the gas heating rate through chemical reactions was calculated as

$$Q_R = k_5[N_e][N_2(X)]\Delta E_5 + [N_2(A)]^2(k_{13}\Delta E_{13} + k_{14}\Delta E_{14})$$
$$+ [N_e]([N_2^+]k_{19}\Delta E_{19} + [N_4^+]k_{20}\Delta E_{20}). \tag{22}$$

The convective plasma cooling due to a gas flow parallel to the anode surface was calculated as [9, 24]

$$Q_C = \left(\frac{5}{2}([N_2(X)] + [N_2(A)] + [N_2(B)] + [N_2(C)] + [N_2(a)] + [N_2^+])\right.$$
$$\left. + \frac{6}{2}[N_4^+] + \frac{3}{2}([N^+] + [N(^4S)] + [N(^2D)] + [N(^2P)])\right)k(T_g - T_\infty)v_F, \tag{23}$$

where $v_F = 2\,u/L$ is the heat removal frequency (u is a characteristic velocity of the gas flow at the anode boundary layer and L a discharge characteristic length along the flow) [9] and T_∞ is the temperature of the gas far from the discharge.

The balance equations for the densities of $N_2(A^3\sum_u^+)$, $N_2(a'^1\sum_u^-)$, $N(^2D)$, $N(^2P)$, $N(^4S)$, N_4^+, N^+ and electrons, in according to the reactions given in Table 1, together with the

Eqs. (10) and (21); were solved numerically by a finite-difference explicit method with the second-order approximation. Once the solution has been obtained, the current density of the discharge was calculated as

$$J = e[\mathrm{N}_e]\mu_e E. \tag{24}$$

Results and Discussion

As mentioned in the Introduction, it was experimentally found a fraction of about 10 % of the main arc current flowing upstream of the arc attachment trough a dark anode boundary layer [8]; thus indicating there the existence of a non-thermal diffuse (glow-like) discharge with a current density $J \sim 1$ A/cm^2 for the present conditions (arc current of 100 A, anode of 5 mm diameter and 25 mm in length). To find the discharge conditions previous to the arc reattachment, the stationary solution was obtained, from reasonable initial values, by assuming a constant voltage drop of about 100 V (see Fig. 1) across a thick anode boundary layer of 1–2 mm [2, 4, 25]. The characteristic frequency of convective heat removal was taken as $\nu_F = 2\ u/L = 2 \times 10^5$ s^{-1} ($u = 100$ m/s [7] and $L = 0.001$ m representing a typical diameter for a constricted discharge). For a relatively broad range of constant electric field values investigated [$(0.5–1) \times 10^5$ V/m], the results showed the presence of a non-thermal discharge with rather high gas temperature ($T_g \sim 4000$ - K $< T_v \sim 4000$–6000 K $< T_e \sim 6500$–8000 K) and a relatively high electron density (of the order of 10^{17}–10^{18} m^{-3}) mainly due to associative ionization. The discharge current density varied in the range 1–5 A/cm^2, whereas the reduced electric field was about 30–40 Td. These values are in according to those reported for atmospheric pressure glow-like discharges in molecular gases [20, 26]. For E/N larger than about 40 Td (corresponding to $E > 0.8 \times 10^5$ V/m), no stationary solution was found; thus indicating that the arc reattachment is essentiality a threshold process. Although the characteristic frequency of convective heat removal has influence on this E/N threshold value, it only plays a minor role in the developing of the reattachment due to the velocity of the process. Under the considered conditions the gas cooling characteristic time ($\equiv \nu_F^{-1}$) is about 5 μs, comparable to the whole reattachment process time during which it is expected that T_g significantly grows. However, since a substantial discharge cooling would require between 5 and 10 cooling characteristic times, the gas discharge cooling only plays a minor role during the reattachment build up.

In order to investigate the kinetic mechanism of the arc restrike, the above quoted stationary (initial) values were perturbed by applying a voltage ramp to simulate the linear increases of the voltage value across the anode boundary layer due to the forward movement of the arc root (as shown in Fig. 1). During the calculations it was assumed that $T_\infty = 4000$ K, in according to the calculated discharge conditions previous to the arc reattachment. The simulation results are presented in Figs. 3, 4, 5, 6 and 7.

Figure 3 presents the temporal behavior of the characteristic plasma temperatures in the discharge. Note that the strong increase of the vibrational temperature of the molecule leads to a further increase in the gas temperature due to the V–T relaxation process that in turn produces an increase of the V–T relaxation rate (due to the strong exponential dependence of this rate coefficient on the gas temperature) which accelerates the gas temperature raise itself. This behavior corresponds to the vibrational instability mode [12] with a whole developing time of ~ 120 μs in the studied conditions.

Fig. 3 Time evolution of the characteristic temperatures of the plasma during the discharge
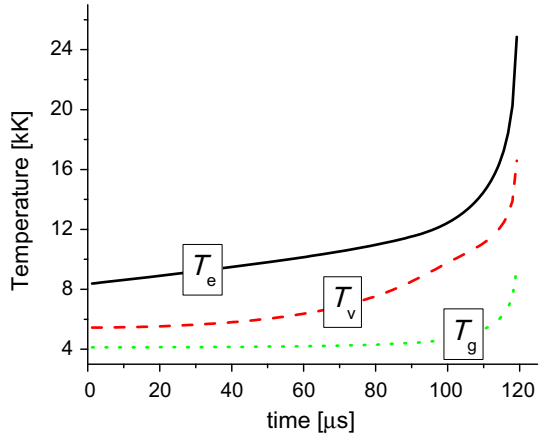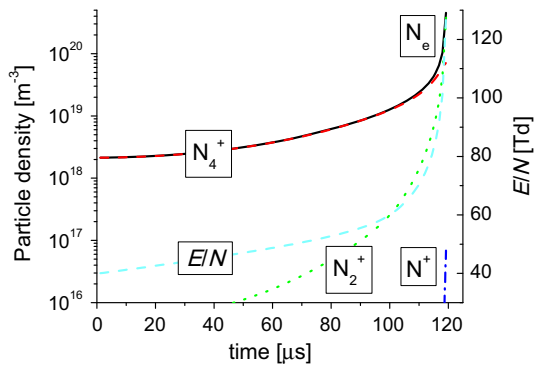

Fig. 4 Time evolution of charged particle densities of the plasma during the discharge

The charged particle densities together with the reduced electric field of the discharge are presented in Fig. 4. It is observed that the complex N_4^+ ion (associative ionization mechanisms R10–R11) is dominant during most of the voltage ramp; but with the sudden increase in the reduced electric field (mainly owing to the decreasing in the gas density) that ion is progressively replaced by N_2^+ (mainly created by electron impact ionization R6).

The calculated mechanisms for the gas heating considered in Eq. (21) are presented in Fig. 5. At $E/N < 80$–100 Td, most of the electron energy is transferred to vibrational modes and then to gas temperature mainly through the mechanism of V–T relaxation. For larger values of E/N, due to the strong vibrational non-equilibrium ($T_v \gg T_g$) state of the molecules, the an-harmonic (V–V)–T relaxation of nitrogen molecules comes into operation in addition with the electronic E–T energy relaxation mechanism Q_R (the so called "fast" gas heating [13–16]) thus producing a further intensification of the gas heating.

The contributing terms for the "fast" heating are presented in Fig. 6. The major contribution for Q_R comes from the quenching of the metastable state $N_2(A^3\sum_u^+)$ in the reaction R13. The other mechanisms (quenching reaction R14, dissociation via pre-dissociation states R5 and recombination R19–R20) play only a minor role in the discharge.

Fig. 5 Time evolution of the considered gas heating mechanisms: V–T relaxation, anharmonic $(V$–$V)$–T relaxation and E–T relaxation (the "fast" gas heating)
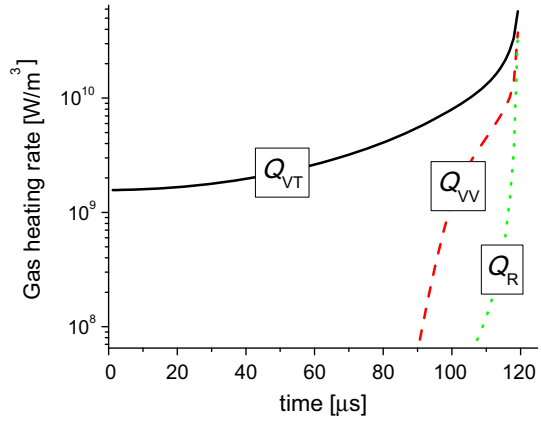

Fig. 6 Time evolution of the gas "fast" heating contributing terms: quenching reactions R13–R14, dissociation R5 and recombination electron–ion R19–R20
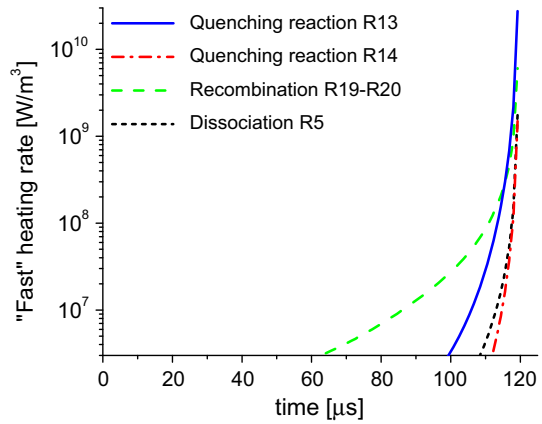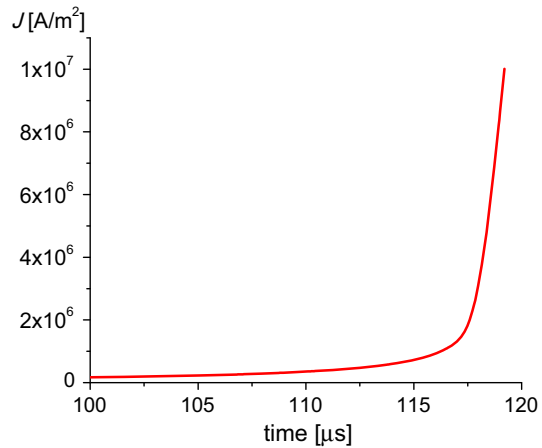

Fig. 7 Detailed time evolution of the current density during the final stage of the discharge

Finally the time evolution of the current density is shown in Fig. 7 with a broader temporal scale (for a time >100 μs). The sharp increase of the gas heating rate during the last few μs of the vibrational instability (as shown Fig. 5) give rises to a sudden transition from a diffuse (glow-like) discharge to a constricted arc with a high current density ($\sim 10^7$ A/m^2). This sudden increase in the current density gives rise to a new anode attachment closer to the cathode thus causing the decay of the old one.

A global analysis of Figs. 3, 4, 5, 6 and 7 shows that the model correctly describes the arc voltage variations showed in Fig. 1.

Conclusions

The present work presented a detailed kinetic analysis of the time-resolved dynamics of the gas heating during the arc reattachment in nitrogen gas in order to understand the main processes leading to such a fast reattachment. The model results have shown that:

1. The anode arc reattachment is essentiality a threshold process. For the plasma discharge conditions considered in this work, such a threshold corresponds to a reduced electric field $E/N \sim 40$ Td.
2. The arc reattachment is triggered by a vibrational instability lasting for a time of the order of 100 μs. For $E/N < 80$–100 Td, most of the electron energy is transferred to gas heating through the mechanism of V–T relaxation. For larger values of E/N the anharmonic $(V$–$V)$–T relaxation of nitrogen molecules becomes relevant together with the electronic E–T energy relaxation mechanism, thus producing a further intensification of the gas heating.
3. The sharp increase of the gas heating rate during the last few μs of the vibrational instability give rises to a sudden transition from a diffuse (glow-like) discharge to a constricted arc with a high current density ($\sim 10^7$ A/m^2). This sudden increase in the current density gives rise to a new anode attachment closer to the cathode thus causing the decay of the old one.

References

1. Boulos M, Fauchais P, Pfender E (1994) Thermal plasmas, fundamentals and applications, vol 1. Plenum Press, New York and London
2. Fauchais P (2004) J Phys D Appl Phys 37:R86–R108
3. Vilotijevic M, Dacic B, Bozic D (2008) Plasma Sources Sci Technol 18:8
4. Fauchais P, Vardelle A (2000) Plasma Phys Control Fusion 42:B365–B383
5. Prevosto L, Kelly H, Mancinelli B (2013) Rev Sci Instrum 85:7
6. Moreau E, Chazelas C, Mariaux G, Vardelle A (2006) J Therm Spray Technol 15:524–530
7. Trelles JP, Heberlein JVR, Pfender E (2007) J Phys D Appl Phys 40:5937–5950
8. Heberlein J, Mentel J, Pfender E (2010) J Phys D Appl Phys 43:31
9. Raizer YP (1991) Gas discharge physics. Springer, Berlin
10. Nemchinsky V (2014) IEEE Trans Plasma Sci 42:4026–4030
11. Capitelli M, Ferreira CM, Gordiets BF, Osipov AI (2000) Plasma kinetics in atmospheric gases. Springer, New York

12. Fridman A, Kennedy L (2004) Plasma physics and engineering. Taylor & Francis, New York
13. Popov NA (2001) Plasma Phys Rep 27:886–896
14. Popov NA (2011) J Phys D Appl Phys 44:16
15. Mintoussov EI, Pendleton SJ, Gerbault FG, Popov NA, Starikovskaia SM (2011) J Phys D Appl Phys 44:13
16. Aleksandrov NL, Kindysheva SV, Nudnoval MM, Starikovskiy AY (2010) J Phys D Appl Phys 43:19
17. Boeuf JP, Kunhardt EE (1986) J Appl Phys 60:915–923
18. Hagelaar GJH, Pitchford LC (2005) Plasma Sources Sci Technol 14:722–733
19. Bacri J, Medani A (1982) Physica C 112:101–118
20. Benilov MS, Naidis GV (2003) J Phys D Appl Phys 36:1834–1841
21. Gordiets BF, Ferreira CM, Guerra VL, Loureiro J, Nahorny J, Pagnon D, Touzeau M, Vialle M (1995) IEEE Trans Plasma Sci 23:750–768
22. Raizer YP, Shneider MN, Yatsenko NA (1995) Radio-frequency capacitive discharges. CRC, Boca Raton
23. Cao YS, Johnsen R (1991) J Chem Phys 95:7356–7359
24. Shneider MN, Mokrov MS, Milikh GM (2012) Phys Plasmas 19:4
25. Wutzke SA, Pfender E, Eckert ERG (1967) IAAA J 5:707–714
26. Prevosto L, Kelly H, Mancinelli B, Chamorro JC, Cejas E (2015) Phys Plasmas 22:9
27. Brunet N, RoccaSerra J (1985) J Appl Phys 57:1574–1581
28. Popov NA (2009) Plasma Phys Rep 35:436–449
29. Nadler I, Rosenwaks S (1985) J Chem Phys 83:3932–3940
30. Piper LG (1988) J Chem Phys 88:231–239
31. Guerra V, Loureiro J (1997) Plasma Sources Sci Technol 6:361–372
32. Kossyi IA, Kostinsky AY, Matveyev AA, Silakov VP (1992) Plasma Sources Sci Technol 1:207–220
33. Bourdon A, Vervisch P (1996) Phys Rev E 54:1888–1898